Nano Today 54 (2024) 102096

Contents lists available at ScienceDirect

Nano Today

journal homepage: www.elsevier.com/locate/nanotoday

Targeting neutrophils potentiates hitchhiking delivery of drugs and agonists for postsurgical chemo-immunotherapy

Zhiliang Gao [a,1], Ning Wang [a,1], Yuan Ma [b,1], Hongning Sun [a], Mengqi Li [a], Yunlu Dai [c], Xinyi Jiang [d], Shilei Ni [b], Jingcheng Hao [a], Jiwei Cui [a,*]

[a] Key Laboratory of Colloid and Interface Chemistry of the Ministry of Education, School of Chemistry and Chemical Engineering, Shandong University, Jinan, Shandong 250100, China
[b] Department of Neurosurgery, Qilu Hospital and Institute of Brain and Brain-Inspired Science, Cheeloo College of Medicine, Shandong University, Jinan, Shandong 250012, China
[c] Faculty of Health Sciences, University of Macau, 999078, Macao Special Administrative Region of China
[d] Department of Pharmaceutics, School of Pharmaceutical Sciences, Cheeloo College of Medicine, Shandong University, Jinan, Shandong 250012, China

ARTICLE INFO

Keywords:
Liposomes
Hitchhiking delivery
Immunogenic cell death
STING
Chemo-immunotherapy

ABSTRACT

Tumor resection is usually associated with tumor recurrence due to the residual tumor cells. Improving the localized accumulation of therapeutics at the surgical sites is a promising approach for the inhibition of tumor recurrence and metastasis. Herein, we report an in situ hitchhiking strategy for postsurgical tumor therapy via targeting of therapeutics-loaded liposomes to neutrophils (NEs). Anticancer drug Active Ingredient (DOX) and non- nucleotide stimulator of Active Ingredient genes (STING) agonist SR-717 are encapsulated into liposomes followed by surface modification with anti-Ly6G antibodies, which can target NEs in situ in blood stream for hitchhiking delivery to the postsurgical inflamed tumor sites. The delivered DOX can inhibit the growth of residual tumor cells and trigger the tumor immunogenic cell death (ICD) for tumor-specific immunity, while SR-717 can facilitate dendritic cell maturation and enhance antitumor immunity. Consequently, the in situ NE-hitchhiking delivery of therapeutics can efficiently suppress tumor recurrence and metastatic melanoma growth after tumor resection, which circumvents the complex ex vivo processes of separation, engineering, and refusion of leukocytes and represents a targeted delivery strategy for postsurgical cancer chemo-immunotherapy.

Introduction

Chemotherapy is one of the most used approaches to inhibit tumor recurrence and metastasis after postsurgical cancer treatment, but it is usually hampered by its weak bioavailability, undesirable off-targeting, and serious side effects.[1,2] In order to increase the delivery efficacy, improving localized accumulation of therapeutics at the postsurgical sites is highly desirable.[3–5] Cellular hitchhiking of therapeutics has been proven to be an efficient approach to improve drug delivery efficacy. For example, surgical resection of tumors is typically associated with local inflammation and simultaneous release of inflammatory factors (e.g., interleukin-8, IL-8 and tumor necrosis factor α, TNF-α).[6–10] As a result of inflammatory stimulation, leukocytes (e.g., neutrophils, NEs) can rapidly proliferate and migrate to the inflammatory sites efficiently.[11,12] This strategy typically involves the separation of leukocytes from blood, binding of therapeutics onto leukocytes ex vivo, and reinfusion of leukocytes into blood stream for hitchhiking delivery.[13–16] However, the ex situ processing of leukocytes suffers from some challenges, such as the short lifetime of NEs and complex processes.[17,18] In contrast, the in situ hitchhiking strategy via targeting of therapeutics to leukocytes in blood stream can overcome the drawbacks of ex situ processing, which is more favored for practical applications.[19,20] In addition, NEs are the most abundant type (40–75%) of leukocytes compared to other immune cells (e.g., macrophages) in blood, which is vital to improve the in situ NE-hitchhiking delivery efficacy [18].

The delivered chemotherapeutic drugs (e.g., Active Ingredient, DOX) can not only result in the tumor cell apoptosis but also induce immunogenic cell death (ICD) to activate antitumor immune responses.[21–26] ICD usually involves express calreticulin (CRT) on the tumor cell surface, release high mobility group box 1 (HMGB1) from the nucleus, and

* Corresponding author.
E-mail address: jwcui@sdu.edu.cn (J. Cui).
[1] These authors contributed equally to this work

https://doi.org/10.1016/j.nantod.2023.102096
Received 12 August 2023; Received in revised form 16 November 2023; Accepted 29 November 2023
Available online 8 December 2023

secrete adenosine triphosphate (ATP). These signals can induce a tumor specific immune reponse, act as a tumor vaccine, to kill the residual tumor cells.[26] Furthermore, it has been reported that the cytosolic dsDNA released from the damaged tumor cells can also activate the stimulator of Active Ingredient genes (STING) pathway to produce Active Ingredient β (IFN-β), which plays an important role in enhancing the presentation of tumor-specific antigens on dendritic cells (DCs) and cross-priming antitumor T cells for adaptive immunity.[27–31] However, the endog-enous immune responses induced by ICD are usually insufficient to effectively suppress the tumor recurrence and metastasis, especially after tumor resection.[32–36] Alternatively, exogenous activation by STING agonists (e.g., cyclic GMP-AMPP) has been proven to be an effi-cient way for the activation of innate immune response to enhance immunotherapy efficacy.[37,38] However, cyclic dinucleotides (CDNs) based STING agonists are hydrophilic negative charged small molecules and easily degraded by enzyme, leading to the limited activation of STING pathway in target tissue.[39–41] Non-nucleotide STING agonists (e.g., SR-717 and MSA-2) have shown their potential for the activation of STING pathway, which could overcome the limitation of instability of CDNs-based agonists.[42,43].

In this work, we report a NE-hitchhiking system to deliver chemotherapeutic drugs (i.e., DOX) and STING agonists (i.e., SR-717) to the postsurgical sites for the inhibition of tumor recurrence and metastatic tumor growth. After tumor resection, inflammatory factors are released and stimulate recruitment of NEs. The subsequent intravenous admin-istration of liposomes loaded with DOX and SR-717 and functionalized with anti-Ly6G antibodies result in the targeting of liposomes to NEs for hitchhiking towards postsurgical sites. The delivered DOX induces ICD of the residual tumor cells after tumor resection, which combines with SR-717 to simultaneously elicit the tumor-specific T-cell immunity via activating the STING pathway (Scheme 1). The combination of anti-cancer drugs and STING agonists result in a significant decrease in tumor recurrence and metastatic tumor growth, as well as an increase in survival time of mice. These findings highlight the advances of in situ NE-hitchhiking system to enhance delivery efficacy and improve tumor immune microenvironments against tumor recurrence and metastatic tumor growth.

Results

Preparation and characterization of liposomes

Liposomes composed of hydrogenated soybean phosphatidylcholine (HSPC), cholesterol, and distearoyl-sn-glycero-3-phosphoethanolamine-PEG2000 (DSPE-PEG2000) (molar ratio of 56:39:5) were prepared by a film-dispersion method.[44] For drug encapsulation, DOX was loaded by a transmembrane ammonium sulfate gradient method, which was based on the exchange of the DOX with ammonium ions. SR-717 was loaded in hydrophobic phospholipid bilayers during the liposome formation. To obtain the liposomes that can target to NEs, biotin-conjugated anti-Ly6G antibodies were functionalized on liposomes based on biotin-avidin recognition (Fig. 1a). Liposomes loaded with DOX or SR-717 were defined as LipD and LipS, respectively, while targeted liposomes loaded with DOX or SR-717 were defined as TLipD and TLipS, respectively. The loading of DOX and SR-717 in liposomes was 13.1 and 7.2 wt%, respectively (Figs. S1, S2, Supporting Information). As shown in Fig. 1b,c, the average size of these liposomes was 150 nm and the ζ-potential was about − 15 mV. No significant changes in size and ζ-potential of liposomes were observed before and after anti-Ly6G modification. In addition, the size of the TLipD and TLipS NPs

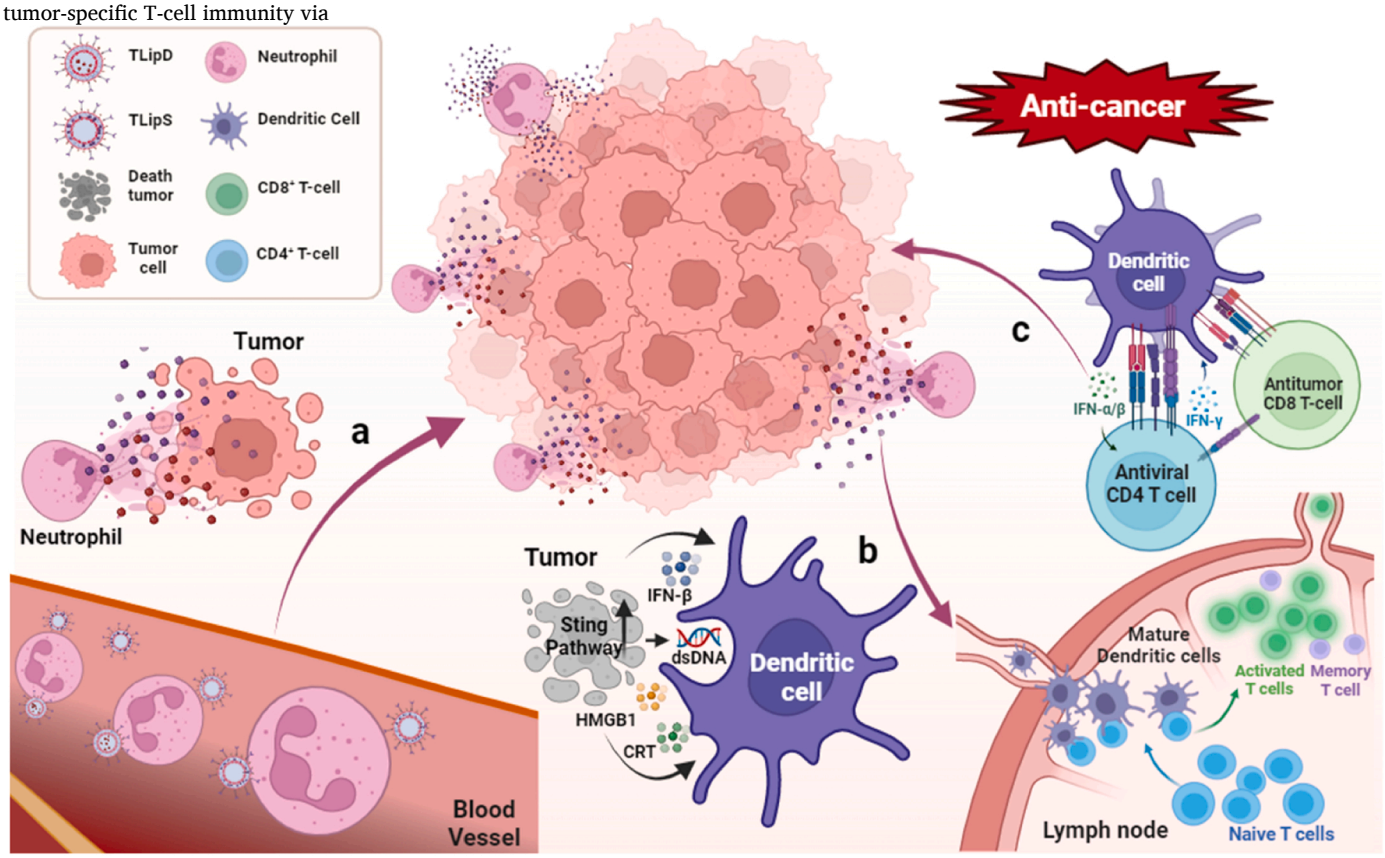

Scheme 1. Schematic illustration of the NE-hitchhiking delivery of targeted liposomes loaded with DOX (TLipD) or SR-717 (TLipS) for synergistic chemo-immunotherapy. (a) Delivery of DOX results in the ICD of residual tumor cells to activate antitumor immune responses. (b) The cytosolic dsDNA from the apoptosis cells and the delivered SR-717 activate the STING pathway to produce IFN-β in both cancer cells and DCs, which can further induce DC maturation. (c) Maturated DCs active T cells to enhance antitumor immunity.

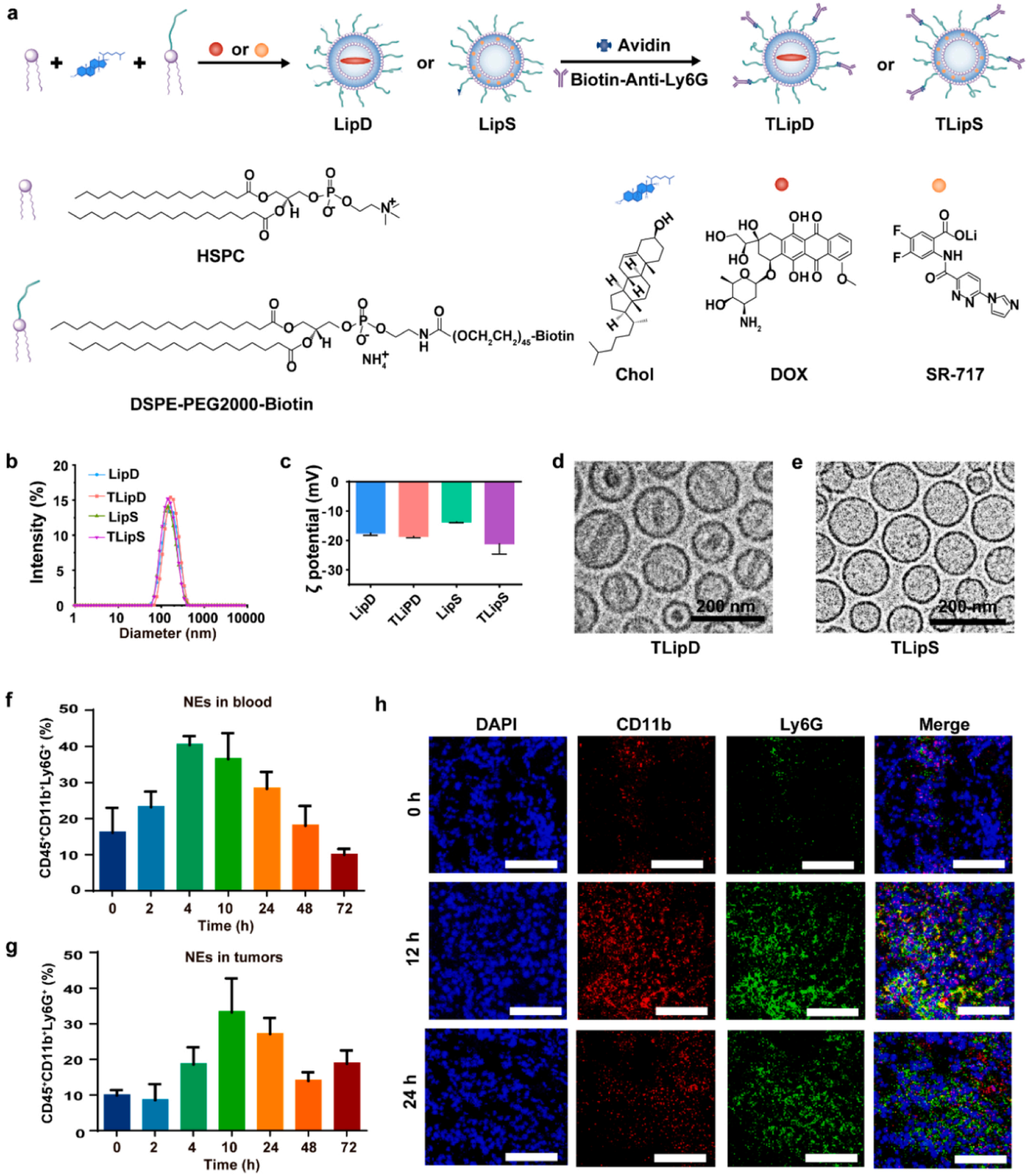

Fig. 1. (a) Schematic illustration of the preparation of TLipD and TLipS, and the chemical structures of lipids (HSPC, DSPE-PEG2000-Biotin and cholesterol), DOX, and SR-717. (b) Size and (c) ζ-potential of LipD, TLipD, LipS and TLipS. Cryo-TEM images of (d) TLipD and (e) TLipS. Quantitative analysis of NEs ($CD11b^+Ly6G^+$) of $CD45^+$ leukocytes in (f) blood and (g) tumor tissues at the indicated time points. The tumors of B16 tumor-bearing mice were surgically removed on Day 8 post-inoculation. Blood and residual tumor tissues were harvested for the detection of NEs by using flow cytometry at predetermined time points (2, 4, 10, 24, 48, and 72 h postsurgery). (h) Immunofluorescence images of NE infiltration in the tumor tissues at 12 and 24 h postsurgery. The tissues were stained with DAPI (blue), anti-CD11b (red), and anti-Ly6G (green). Scale bars are 100 μm. Data are presented as the mean ± SD (n = 3).

did not significantly change after incubating with DPBS and culture medium for 10 days, indicating their good stability (Fig. S3). The morphology of TLipD and TLipS was examined by cryo-transmission electron microscopy (cryo-TEM), which demonstrated hollow vesicle structures of the liposomes (Fig. 1d,e). The formed crystalline nanorods indicated the successful encapsulation of DOX.

Inflammation-induced proliferation and trafficking of NEs

NEs in blood and tumor sites were analyzed at different time points using flow cytometry. The gating strategies and representative flow cytometry analysis are shown in Figs. S4-**7** (Supporting Information). [16] A significant increase in NEs ($CD45^+CD11b^+Ly6G^+$) in blood was observed within 48 h postsurgery and peaked at 4–10 h. In contrast, the peak of NEs at tumor sites was delayed to 10–24 h (Fig. 1f,g), which could be due to the recruitment of NEs from blood circulatory system to tumor inflammatory sites. NE accumulation in the tumor tissues was also visualized by immunostaining of Ly6G and CD11b after tumor resection at representative time points. Both red (CD11b) and green (Ly6G) fluorescence signals peaked at 12 h (Fig. 1h), which is consistent with the flow cytometry results. These results indicate that the proliferation of NEs in blood and recruitment of NEs at tumor sites were due to the surgery-induced inflammation, which provides a potential for NE-hitchhiking delivery.

Targeting of liposomes to NEs

Mouse blood from healthy mice was collected and lysed to remove erythrocytes, followed by incubation with LipD and TLipD to analyze the cell targeting of liposomes. The NE targeting of TLipD was verified by flow cytometry, where the mean fluorescence intensity (MFI) of the TLipD group was significantly higher than that of the LipD group (Figs. S8-S10, Supporting Information). Confocal laser scanning microscopy (CLSM) images also show the presence of DOX (red) in NEs (green), which indicates the specific targeting of TLipD to NEs expressed with Ly6G (Fig. S11, Supporting Information). In contrast, weak DOX fluorescence signals were found in NEs for the LipD group. Therefore, surface modification of anti-Ly6G antibodies affords liposomes that specifically target to NEs. To further verify the in vivo targeting and delivery of DOX-loaded liposomes to NEs, whole blood and tumor tissues were collected and processed at the predetermined time after tumor resection and injection of liposomes, followed by analyzing the NE association of LipD and TlipD with flow cytometry. As a result, TLipD group resulted in 5.7- and 3.5-fold higher NE association than that of LipD group in blood and tumor tissues, respectively, which indicates the well in vivo targeting ability of the anti-Ly6G functionalized liposomes (Fig. 2a-c).

Ex vivo imaging of tumor tissues was examined to investigate the targeted delivery of liposomes. For fluorescence imaging, Active Ingredient green (ICG) as a model drug was loaded into Lip and TLip (denoted as LipICG and TLipICG, respectively). As shown in Fig. 2d,e TLipICG showed higher tumor accumulation than LipICG and maintained the fluorescence intensity at tumor sites even after 24 h postsurgery, which indicated the well accumulation and retention of TLipICG. The targeted delivery of liposomes to postsurgical tumor sites was further evaluated by immunofluorescence staining assay. As shown in Fig. 2f and **S12** (Supporting Information), the accumulation of DOX in the TLipD (nonsurgery) group was similar to the LipD (postsurgery) group, while twice more tumor accumulation of DOX was observed in the TLipD group at 12 h postsurgery compared to that of the LipD group, which indicates that the acute phase of inflammation after tumor resection is of benefit to the transportation and accumulation of TLipD. These results demonstrate that tumor surgery induced local inflammation and NEs with anti-Ly6G functionalized liposomes migrated to inflammatory sites, followed by release of the carried cargos to the postsurgical tumor sites.

Drug delivery and immune activation in vitro

The cytotoxicity of TLipS and TLipD against B16 cells was assessed by a 3-(4,5)-dimethylthiahiazo(-z-y1)− 2,5-di-phenytetrazoliumromide (MTT) assay and the live/dead cell imaging. After incubation of B16 cells with TLipS for 48 h, negligible cytotoxicity of TLipS was observed, even when the equivalent SR-717 concentration was 20 μg/mL. TLipD and TLipDS (both TLipD and TLipS) groups resulted in similar cell cytotoxicity with an IC50 of 8.8 μg/mL (Fig. 2g), which was further confirmed by live/dead cell imaging (Fig. S13, Supporting Information). The intercellular transport of drugs from NEs to tumor cells was investigated by co-culture of TLipD-targeted NEs and B16 cells in the presence of phorbol myristate acetate (PMA), which was typically used to mimic inflammatory factors for the formation of neutrophil extracellular traps (NETs).[6] As a result, DOX was delivered into B16 cells (Fig. 2h). This could be due to the formation of NETs in the presence of PMA stimulation, which induced the disintegration of the NE plasma membrane and subsequent release of TLipD. In contrast, a weak DOX fluorescence signal was found in B16 cells when the NEs were not stimulated by PMA (Fig. S14, Supporting Information).

The effect of DOX on the induction of ICD was investigated by measuring the release of high mobility group box 1 (HMGB1) and the expression of CRT, which are typical indicators for ICD,[22] after incubation of B16 cells with therapeutics-loaded liposomes. Enzyme linked immunosorbent assay (ELISA) measurements showed that the TLipD and TLipDS groups could induce a 2.0-fold and 1.8-fold higher release of HMGB1 from the nuclei than that of the TLipS group (Fig. 2i). Flow cytometry analysis demonstrated that TLipD and TLipDS groups resulted in a 1.3-fold higher expression of CRT than that of the TLipS group (Fig. 2j), which were confirmed by CLSM images that higher green fluorescence signals (CRT-FITC) were observed in the TLipD and TLipDS groups than that of the TLipS group (Fig. 2k). These results indicate that DOX-loaded liposomes can effectively induce ICD, which is promising to activate immune responses.

To investigate the maturation of bone marrow-derived dendritic cells (BMDCs) induced by ICD or agonists in vitro, BMDCs were incubated with the culture medium of B16 cells after different treatments with TLipD, TLipS or TLipDS. The percentage of the matured BMDCs ($CD11c^+CD80^+CD86^+$) was examined by flow cytometry. As shown in Fig. 2l and **S15**, Supporting Information, TLipD and TLipS groups resulted in 1.5- and 1.4-fold BMDC maturation, respectively, compared to the PBS group (~29%), while TLipDS group could significantly promote the BMDC maturation (~51%) compared to the TLipD and TLipS groups. Moreover, the cytokines produced by BMDCs were measured by ELISA kits. The TLipDS group showed improved secretion of interleukin-6 (IL-6, Th2-type cytokine) and tumor necrosis factor α (TNF-α Th1-type cytokine) (Fig. 2m,n). The above results indicate that the co-delivery of DOX and SR-717 can efficiently promote BMDC maturation and cytokine secretions.

Inhibition of tumor recurrence and metastatic tumor growth

The inhibition of tumor recurrence was evaluated on postsurgical B16 tumor-bearing mice, the schedule of which is shown in Fig. 3a. Mice were intravenously injected with PBS, TLipS, TLipD, LipDS and TLipDS at 4 h postsurgery. The body weight and tumor volume were monitored every 2 days. As a result, no significant changes were founded during the treatments (Fig. S16, Supporting Information), indicating the well biocompatibility of liposome-based therapeutics, which were also verified by the analysis of alanine transaminase (ALT), alkaline phosphatase (ALP), carbamide (UREA), and creatinine (CREA) in blood (Fig. S17, Supporting Information). Compared with PBS group, TLipS, TLipD and LipDS groups could partially inhibit the tumor growth (Fig. 3b,c). Notably, tumor recurrence and growth were well controlled by the TLipDS group until to 44 d, which should be attributed to the effective drug accumulation and synergy of chemo-immunotherapy (Fig. 3d). The

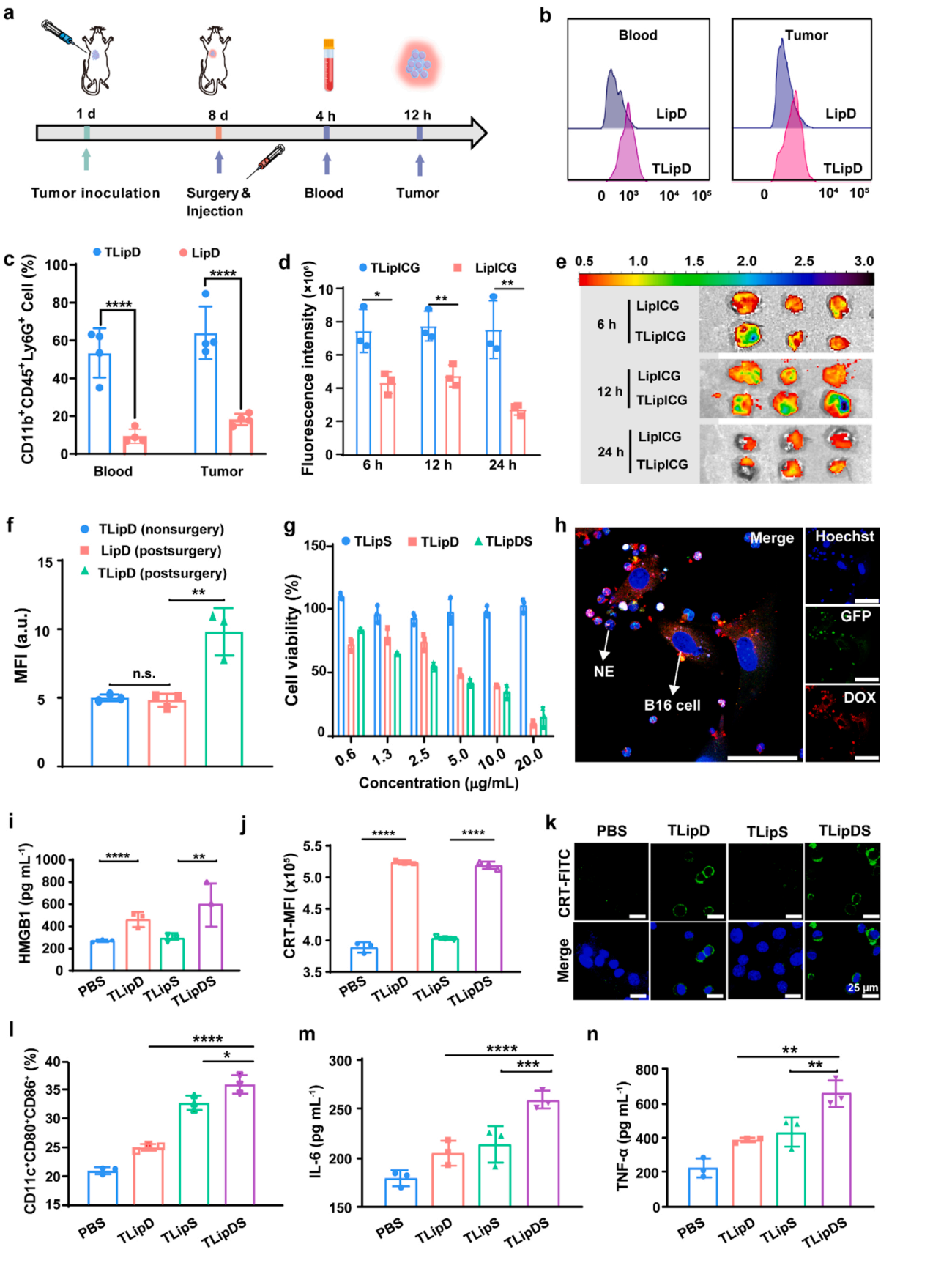

(caption on next page)

Fig. 2. (a) Time schedule for the evaluation of in vivo targeting of liposomes to NEs on a B16 tumor-bearing mouse model. C57BL/6 mice were subcutaneously injected with B16 cells on Day 1, followed by surgical removal of tumors (80%) on Day 8 and intravenous injection of TlipD and LipD. At 4 and 12 h postinjection, NEs in blood and tumor were labeled with CD45, CD11b and Ly6G for further analysis, respectively. Representative flow cytometry plots (b) and statistical data (c) of NEs after incubation with TLipD and LipD. Data are presented as the mean ± SD (n = 4). (d) Qualitative fluorescence analysis and (e) ex vivo images of tumor tissues after the injection of LipICG or TLipICG at the indicated time points (6, 12 and 24 h). (f) Distribution of LipD and TLipD in tumor tissues with or without surgical resection. (g) Cell viability of B16 cells after incubation with TLipS, TLipD or TLipDS for 48 h (equivalent DOX or SR-717 concentration of 0.6, 1.3, 2.5, 5.0, 10.0, and 20.0 μg mL^{-1}). (h) CLSM images of B16 cells after incubation with TLipD-targeted NEs, followed by the treatment with PMA. Green fluorescence protein (GFP) signal was expressed in NEs from GFP transgenic mice. Scale bars are 50 μm. (i) HMGB1 release from B16 cells after incubation with TLipD, TLipDS, or TLipS for 24 h. (j) Flow cytometry analysis and (k) CLSM images of CRT expression on B16 cells. Scale bars are 25 μm. Cell nuclei and CRT were stained with Hoechst 33342 (blue) and FITC-anti-CRT (green), respectively. (l) Flow cytometry analysis of BMDC maturation in vitro. Cytokine secretion of (m) IL-6 and (n) TNF-α from BMDCs, as determined by ELISA. BMDCs were incubated with the culture medium of B16 cells, which were pre-treated with TLipD, TLipDS, or TLipS for 24 h. Data are presented as the mean ± SD (n = 3). Statistically significant differences between groups are identified by one-way ANOVA. * $P < 0.05$, * * $P < 0.01$, * ** $P < 0.001$, * ** * $P < 0.0001$.

survival rate of the TLipDS group reached as high as 80% in 44 d, a much better outcome than that of the LipDS group (three out of ten, 30%) (Fig. 3e). Furthermore, hematoxylin-eosin (H&E) staining, terminal deoxynucleotidyl transferase-mediated dUTP nick-end labeling (TUNEL), and Ki67 immunofluorescence analysis of tumor tissues were examined to investigate the therapeutic activity (Fig. S18, Supporting Information). The TLipDS group resulted in more tumor tissue disruption and tumor cell apoptosis than the other groups, and therefore significantly inhibited the proliferation of tumor cells.

To further evaluate the therapeutic effect of liposome-based therapeutics, metastatic lung tumor models were established, followed by injection of liposomes to investigate the inhibition of tumor growth (Fig. 3f). The mice treated with PBS, TLipS, or TLipD groups showed visible lung tumors as black dots (Fig. 3g). Although the tumor sizes in the LipDS group were smaller than those of TLipS and TLipD groups, the tumors were dispersively distributed in lungs. In contrast, rare tumor dots were observed in the TLipDS group, which indicates that TLipDS could efficiently inhibit the growth of metastatic tumor cells. This should be due to the effective targeted hitchhiking delivery of drugs and agonists for the activation of antitumor immune responses. H&E staining of lung sections and numbers of metastatic tumor nodules further verified the superiority of the TLipDS group for the inhibition of metastatic tumors (Fig. 3h,i). Furthermore, the survival time of mice in the TLipDS group was significantly prolonged compared to other groups (Fig. 3j).

Activation of STING pathway

Cancer cell-intrinsic STING pathway, which can be activated by chemotherapeutics-induced ICD, plays a vital role in antitumor immunity. DOX is expected to cause ICD and release of tumor-specific antigens, which together with SR-717 can activate the STING pathway and stimulate DC maturation (Fig. 4a). To investigate the effect of DOX and SR-717 on cGAS/STING signaling in tumor-bearing mice, the levels of cGAS, STING, TBK1 and IRF3, as well as phosphorylation levels of STING, TBK1 and IRF3 were examined by western blotting. As shown in Fig. 4b,c, the level of cGAS as well as phosphorylation of STING, TBK1 and IRF3 (indicators of STING pathway) were up-regulated in the TLipS, TLipD and LipDS groups, but the activation was weaker than that of the TLipDS group, which was attributed to the efficient accumulation of therapeutics based on targeted NE-hitchhiking strategy and synergetic activation of the co-delivered DOX and SR-717.

To investigate the effect of DOX and SR-717 on the immune microenvironment through the activation of STING pathway, RNA was extracted from tumor tissues after different treatments and the STING pathway related gene expression levels were detected by real-time polymerase chain reaction (PCR). As a result, multiple gene expression levels (i.e., signaling transduction molecules, Active Ingredient related molec-ular, JAK-STAT signaling, STING activates downstream genes and T cell infiltration and function) in the TLipD and TLipS groups were up- regulated (Fig. 4d), indicating that the DOX-induced ICD and SR-717 in tumor tissues played an important role in the activation of STING pathway. For the combination therapy group of TLipDS, most of genes associated with the STING pathway showed a significant up-regulation (Fig. 4d), which was consistent with the Western blot results.

In order to further clarify the effect of TLipDS on the activation of STING-related immune pathways and regulation of immune microenvironment, relevant up-regulated genes were selected and analyzed (Fig. 4e). Active Ingredient regulatory factor 7 (IRF7), as a key transcriptional regulator of type I Active Ingredient (IFN)-dependent immune responses, is vital in the innate immune response. IRF7 can activate both IFN-β and the IFN-α genes by binding to an active ingredient-stimulated response element (ISRE) in their promoters, and regulate the antitumor properties of im-mune cells. The high expression of Ifi16 (as an intracellular DNA sensor mediating IFN-β induction) in the TLipDS group could promote to re-cruit STING to induce IFN-β after DNA stimulation.[45] Compared with TLipD, TLipDS group induced higher secretion levels of NF-κB (Fig. S19, Supporting Information), which demonstrated that STING-TBK1-IRF3/STING-TBK1-NF-κB pathways can be activated by the combination treatment of TLipDS. The treatment of TLipD or TLipDS released immunogenic substances from tumor cells (e.g., DNA) to acti-vate the STING pathway at the tumor sites. SR-717 could further amplify the signals and recruit immune cells, which induced the continuous activation of STING pathway. In addition, gene ontology (GO) analysis showed that the TLipDS group contributed to biological processes associated with the STING pathway (e.g., NF-κB pathways and type I Active Ingredient) , compared to the PBS group (Fig. 4f and **S20,** Supporting Information). Therefore, the combination of DOX and SR-717 plays a crucial role in the activation of the sting pathway for antitumor effects in animals.

To confirm the changes of immune regulatory factors in immunosuppressive microenvironment caused by the activation of STING pathway, pro-inflammatory cytokines of CCL5/RANTES, CXCL10, TNF- α and IFN-β in tumor tissues were analyzed by the ELISA (Fig. 4**g**-j). As a result, the TLipDS group resulted in higher production of immune reg-ulatory factors compared to other groups, which were consistent with the results ontained from Western blot and qRT-PCR. The TLipDS group could effectively relieve immunosuppressive tumor microenvironment by up-regulation of tumor suppressor inflammatory factors. The remodeling of immunosuppressive microenvironments effectively attractes monocytes/macrophages, NK cells and dendritic cells, and promoted the recognition of T cells to inhibit tumor recurrence and metastasis after surgery.

Amelioration of tumor microenvironments

DOX-induced ICD could provide damage-associated molecular patterns (DAMPs) to release a signal of “eat me” (i.e., calreticulin, CRT), accompanied by the release of HMGB1, which can subsequently stimulate DC maturation.[46–48] Furthermore, the activated STING induced by SR-717 could elevate the release of type I IFN, which reinforces tumor-specific antigen presentation on DCs and further activates antitumor T cells for adaptive immunity and improvement of tumor immune microenvironments (Fig. 5a).[49] To demonstrate the antitumor

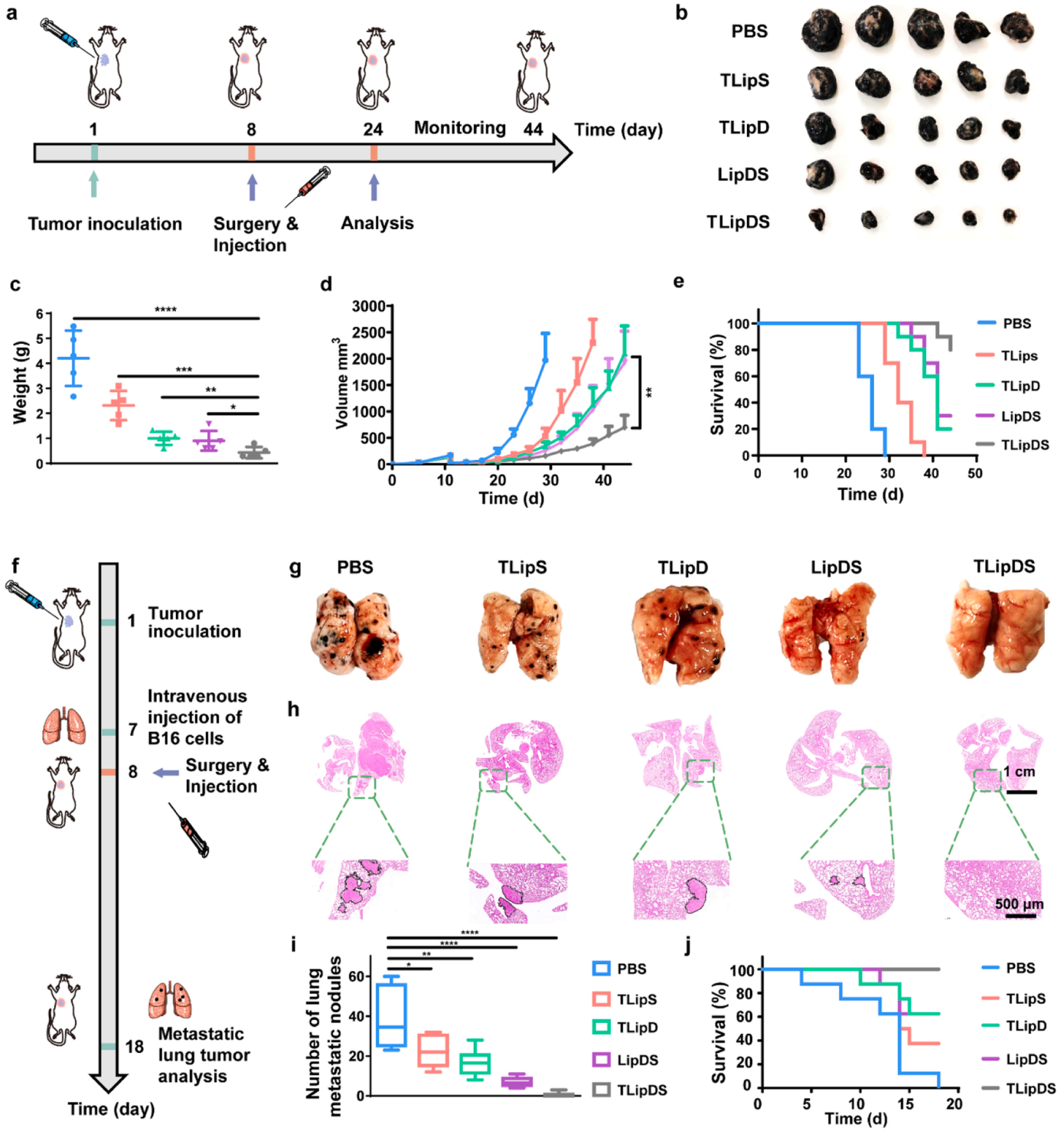

Fig. 3. (a) Time schedule for the establishment and treatment of B16 tumor-bearing mouse models. C57BL/6 mice were subcutaneously injected with B16 cells on Day 1, followed by surgical removal of tumors (80%) on Day 8 and intravenous injection of PBS, TLipS, TLipD, LipDS or TLipDS (DOX or SR-717 dosage of 15 mg/kg). On day 24, five of mice were euthanized to obtain the tumors for further analysis, and other mice were monitored for a longer period of time to study the tumor recurrence and survival rates. (b) Representative photographs of tumors, and (c) tumor weights after treatment with PBS, TLipS, TLipD, LipDS or TLipDS. (d) Tumor growth profiles and (e) survival curves of mice after different treatments. (f) Time schedule for the establishment of subcutaneous B16 tumor models and the inhibition of metastatic lung tumors after tumor resection. C57BL/6 mice were subcutaneously injected with B16 cells on Day 1. B16 cells were intravenously injected in C57BL/6 mice on day 7 for the establishment of metastatic lung tumor models, followed by surgical removal of subcutaneous tumors and intravenous injection of PBS, TLipS, TLipD, LipDS or TLipDS on Day 8 (DOX or SR-717 dosage of 15 mg/kg). Lungs of each group were obtained for further analysis on Day 18. (g) Photographs of lungs. (h) H&E staining images of lung sections after different treatments. (i) Number of metastatic tumor nodules in lungs. (j) Survival curves of mice after different treatments. Data are presented as the mean ± SD (n = 5). Statistically significant differences between groups are identified by one-way ANOVA. * $P < 0.05$, * * $P < 0.01$, * ** $P < 0.001$, * ** * $P < 0.0001$.

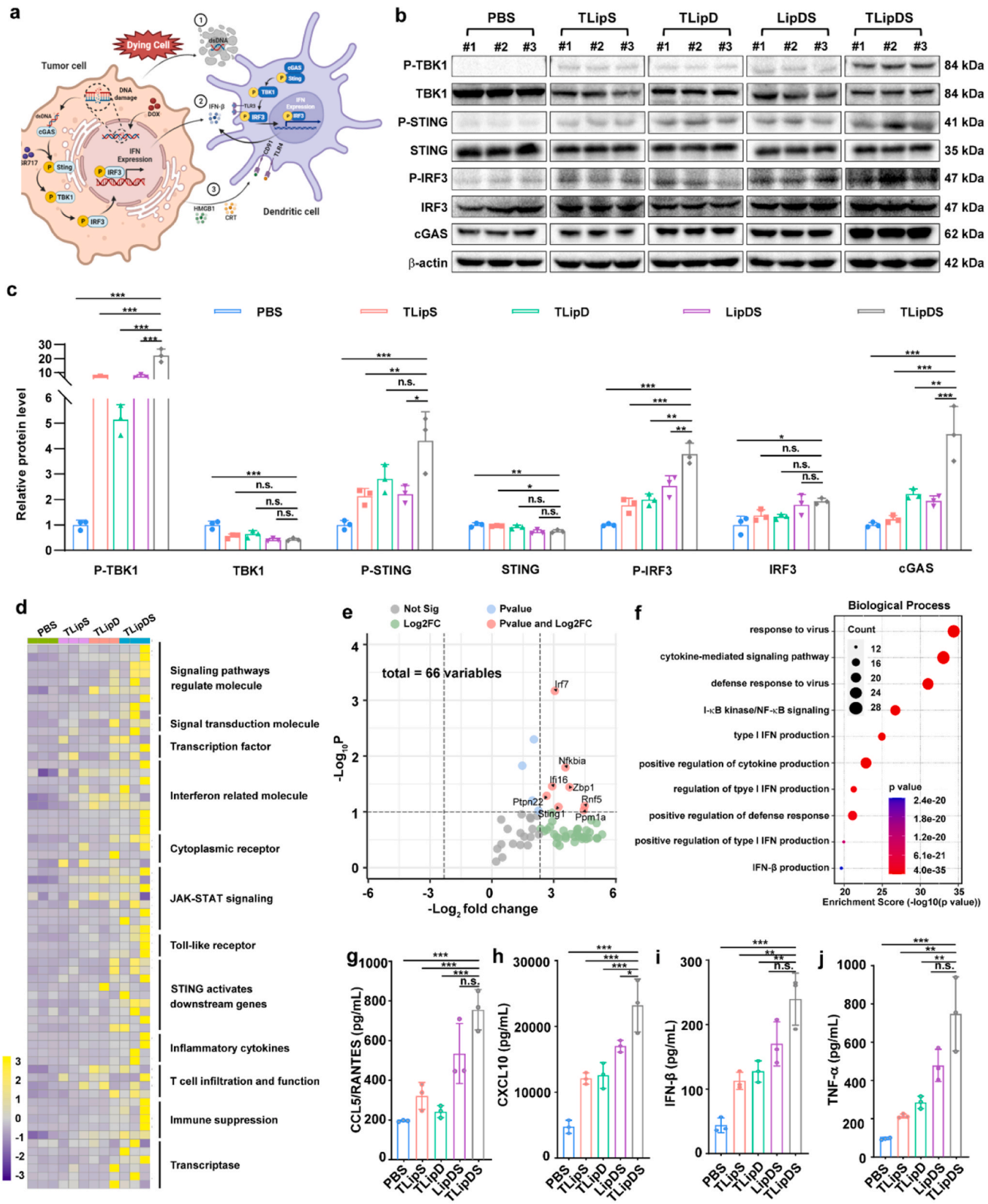

Fig. 4. (a) Schematic illustration of the activation of STING pathway. (b) Western blotting of STING, TBK1, IRF3, cGAS, and phosphorylation of the indicated proteins in the tumor tissues. Data are presented as the mean ± SD (n = 3). (c) Quantification of protein levels from the western blotting results. (d) Changes of gene enrichment after the treatments with PBS, TLipS, TLipD, or TLipDS. (e) Volcano plot of differentially regulated genes related to signaling pathway regulate molecules, Active Ingredient related molecules, cytoplasmic receptors, and STING activating downstream genes (PBS vs TLipDS). (f) Biological process of tumor tissues through GO annotation analysis (PBS vs TLipDS). ELISA analysis of cytokine secretion of CCL5/RANTES (g), CXCL10 (h), IFN-β (i), and TNF-α (j) in tumor tissues. Data are presented as the mean ± SD (n = 3). Statistically significant differences between groups are identified by one-way ANOVA. * $P < 0.05$, * * $P < 0.01$, * ** $P < 0.001$.

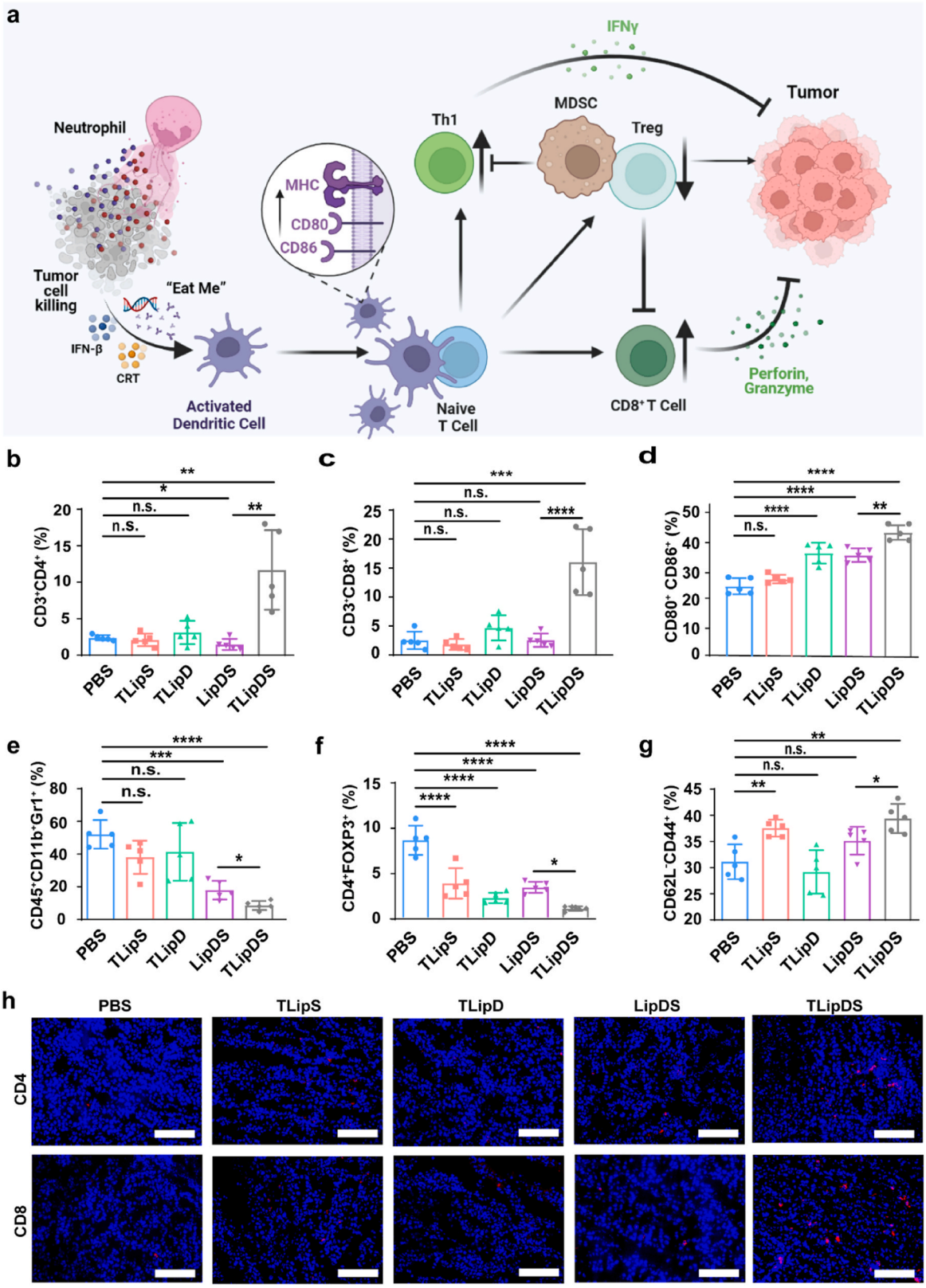

Fig. 5. (a) Schematic illustration showing the changes of immune microenvironments after hitchhiking delivery of DOX and SR-717. Percentages of $CD3^+CD4^+$ (b) and $CD3^+CD8^+$ (c) T cells in tumors after treatments with PBS, TLipS, TLipD, or TLipDS. (d) Percentages of $CD80^+CD86^+$ DCs in total $CD11c^+$ DCs in lymph nodes after the treatments. Percentages of $CD45^+CD11b^+Gr1^+$ (e), $CD4^+Foxp3^+$ (f) and $CD62L^-CD44^+$ (g) T cells in total T cells in tumors. (h) Immunofluorescence images of $CD4^+$ and $CD8^+$ T cells in tumor sections after the treatments. Scale bars are 100 μm. Cell nuclei, $CD4^+$ and $CD8^+$ T cells were stained with DAPI (blue), PE-anti-CD4 (red) and PE-anti-CD8 (red), respectively. DOX fluorescence signal (red) was used to represent the liposome signal. Data are presented as the mean ± SD (n = 5). Statistically significant differences between groups are identified by one-way ANOVA. * $P < 0.05$, * * $P < 0.01$, * ** $P < 0.001$, * ** * $P < 0.0001$.

immunity evoked by ICD and activation of STING pathway, intratumoral infiltration of immune cells was examined. Notably, the TLipDS group induced the highest increase in the abundance of helper T lymphocytes ($CD3^+D4^+$) and cytotoxic T cells ($CD3^+CD8^+$) compared to other groups (Fig. 5b,c and **S21,** Supporting Information). This demonstrates that the presence of targeting molecules and STING agonists is desirable to activate strong immune responses. Since DCs as one of the most important antigen- presenting cells antigen presenting cells can present tumor antigens to $CD8^+$ T cells for the activation and proliferation of antigen-specific T cells to eliminate tumor cells, the maturation level of DCs in tumor draining lymph nodes was investigated for elucidating the mechanism in the combination therapy.[50] The co-delivery of DOX and SR-717 resulted in higher activation levels of DC maturation compared to other groups (Fig. 5d and **S22,** Supporting Information).

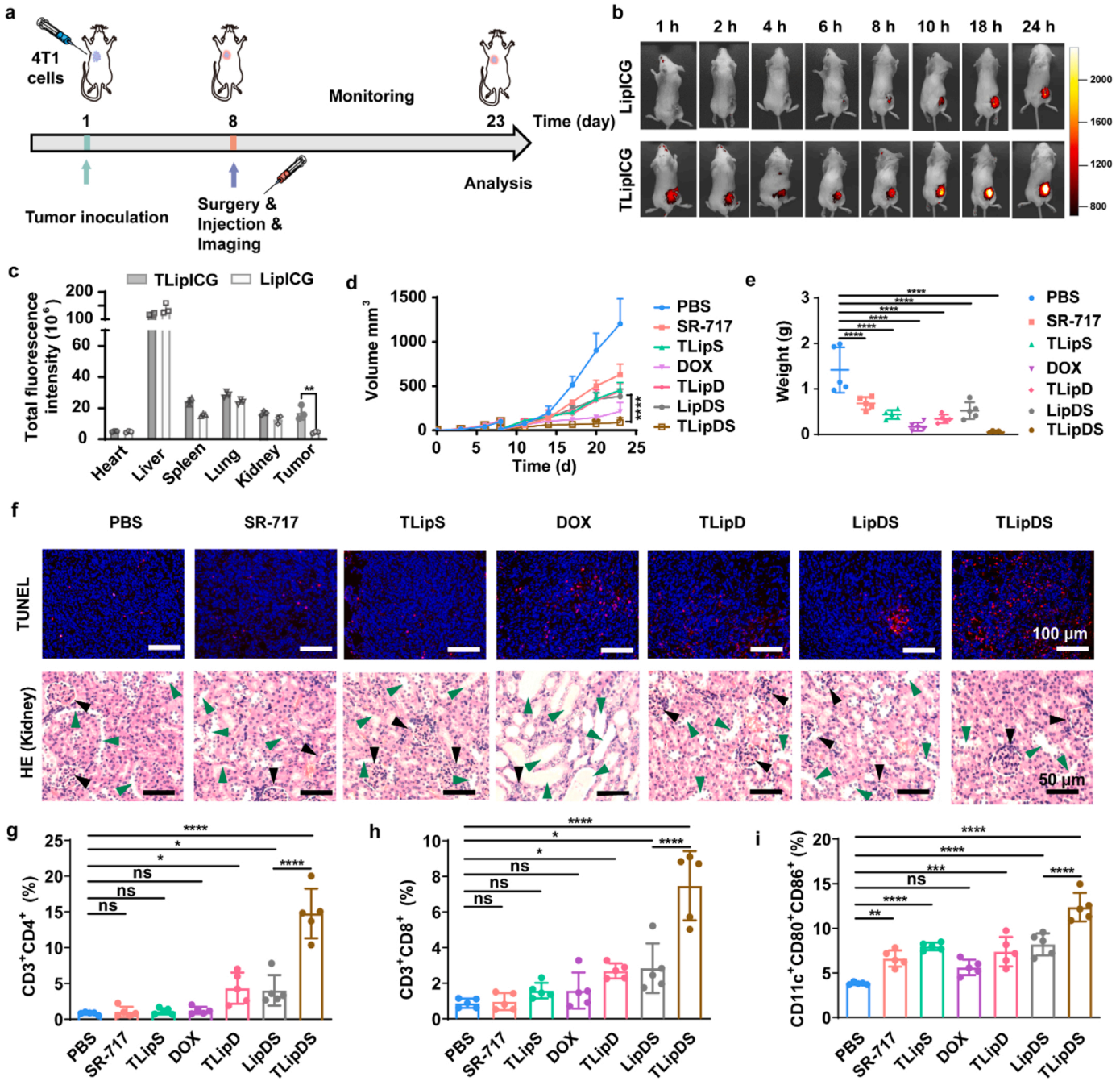

Fig. 6. (a) Time schedule for the establishment and treatment of 4T1 tumor-bearing mouse models. Balb/c mice were subcutaneously injected with 4T1 cells on Day 1, followed by resection of tumors (80%) on Day 8 and intravenous injection of targeted and non-targeted liposomes for imaging and therapy. (b) In vivo fluorescence imaging of the 4T1 tumor-bearing mice after intravenous injection of TLipICG or LipICG at 1, 2, 4, 6, 8, 10, 18, 24 h, respectively. (c) Fluorescence intensity of different organs and tumors ex vivo. Data are presented as the mean ± SD (n = 3). Statistically significant differences between groups are identified by one-way ANOVA. * * $P < 0.01$. (d) Tumor growth profiles after treatments with PBS, SR-717, TLipS, DOX, TLipD, LipDS or TLipDS (DOX or SR-717 dosage of 15 mg/kg). (e) Tumors weight after treatments with PBS, SR-717, TLipS, DOX, TLipD, LipDS or TLipDS. (f) TUNEL staining images of 4T1 tumor tissues and H&E staining images of kidney after different treatments. (black triangle: glomerulus; green triangle: renal tubule). (g,h) Percentages of $CD3^+CD4^+$ and $CD3^+CD8^+$ T cells in tumors after different treatments. (i) Percentages of $CD80^+CD86^+$ DCs in total $CD11c^+$ DCs in lymph nodes after different treatments. Data are presented as the mean ± SD (n = 5). Statistically significant differences between groups are identified by one-way ANOVA. * $P < 0.05$, * * $P < 0.01$, * ** $P < 0.001$, * ** * $P < 0.0001$.

Myeloid-derived suppressor cells (MDSCs) and tumor infiltration of regulatory T cells (Tregs) are vital in the regulation of tumor immunosuppressive microenvironments, which seriously limits antitumor immune responses.[51,52] Notably, co-delivery of DOX and SR-717 led to a remarkably reduced MDSCs (Fig. 5e and **S23,** Supporting Information) and Tregs (Fig. 5**f** and **S24,** Supporting Information), which was important to show the activation of antitumor immunes. It is known that local immunological memory can promote adaptive immunity, which provides long-term immunity against tumor recurrence and distant metastases. To analyze immunological memory induced by the chem-immunotherapy, tumors from the mice treated with different therapeutic groups were collected for flow cytometry analysis. As shown in Fig. 5g and **S25,** Supporting Information, the TLipS and TLipDS groups exhibited a remarkable improvement of effector memory T cells ($CD62L^{-}CD44^{+}$), while no significant differences were observed in the LipDS and TLipD groups compared to the PBS group, which could be due to the less tumor accumulation of drugs and agonists in the non-targeted LipDS group and the absence of agonists in the TLipD group, respectively. The tumor infiltration of helper T cells and effector T cells was confirmed by the immunofluorescence staining of $CD4^{+}$ and $CD8^{+}$ T cells (Fig. 5h), which further proved the improvement of immune microenvironment after the treatment with TLipDS. Taken together, the in situ targeting of TLipDS to NEs for efficient hitchhiking delivery could result in more tumor accumulation of drugs and agonists, which can effectively activate STING signaling pathway and trigger systemic immune responses to improve the tumor immune microenvironment for cancer therapy.

Antitumor effect in 4T1 bearing mice

To further confirm the in situ NE-hitchhiking delivery for postsurgical chemo-immunotherapy, the antitumor efficacy of TLipDS was investigated on the 4T1 tumor-bearing BALB/c mice (Fig. 6a). Tumor accumulation and biodistribution of the TLipICG and LipICG were monitored via fluorescence imaging. Both groups exhibited time-dependent tumor accumulation (Fig. 6b). TLipICG group showed more accumulation of liposomes at tumor sites compared to the LipICG, where the MFI of the tumor in the TLipICG was 1.4-fold higher than that in the LipICG group at 24 h (Fig. 6c and **S26,** Supporting Information). Treatments with SR717, TLipS, TLipD and LipDS showed moderate inhibition of tumor growth. Notably, the TLipDS group demonstrated the best antitumor efficacy among all groups, indicating that NE-hitchhiking targeted delivery of therapeutics at the postsurgical site and combination of chemo-immunotherapy are crucial for the inhibition of tumor recurrence (Fig. 6d,e and **S27,** Supporting Information). H&E staining, Ki67 and TUNEL analysis of tumor tissues further revealed that the targeted chemo-immunotherapy induced necrosis and apoptosis of tumors (Fig. 6f and **S28,** Supporting Information). Remarkably, free DOX group significantly suppressed the growth of tumours compared with the PBS group. However, injection of free DOX was accompanied with severe ascites and weight loss (Fig. S29, Supporting Information). H&E staining in the DOX group resulted in abnormal glomerulus and renal tubule structure, which was due to that DOX could induce the generation of reactive oxygen species and promote the oxidation and senescence of kidney cells.[53,54] On the contrary, DOX-loaded liposomes could significantly reduce the damage of the kidney tissues (Fig. 6f). H&E staining of major organs (heart, liver, spleen, lung and kidney) treated with the PBS, SR-717, TLipS, TLipD, LipDS or TLipDS did not show significant histological changes, indicating their low systematic toxicity (Fig. S30, Supporting Information). The intratumoral infiltration of $CD3^{+}CD4^{+}$ and $CD3^{+}CD8^{+}$ T cells was examined by flow cytometry. The infiltration ratio of $CD3^{+}CD4^{+}$ and $CD3^{+}CD8^{+}$ T cells in the LipDS group was 4.1% and 2.8%, respectively, which was 4.6- and 3.4-fold higher than that of the PBS group, respectively. The targeted TLipDS could further increase the infiltration ratio of $CD3^{+}CD4^{+}$ and $CD3^{+}CD8^{+}$ T cells to 14.9% and 7.5%, which was 3.6- and 2.7-fold higher than that of LipDS group (Fig. 6g,h and **S31,** Supporting Information). The intratumoral infiltration of mature DC were also investigated by flow cytometry, which plays a vital role in antigen presentation to T cells and promotes intratumoral infiltration of cytotoxic T lymphocytes.[55] As a result, SR717, TLipS, DOX, TLipD and LipDS groups facilitated the DC maturation from 5.5% to 8.1%. TLipDS group dramatically promoted the intratumoral DC maturation ratio to 12.3%, which was 3.3- and 1.5-fold higher than PBS and LipDS groups, respectively (Fig. 6i and **S32,** Supporting Information). Overall, the study in the 4T1 tumor model confirmed the efficacy of in situ NE-hitchhiking delivery for postsurgical chemo-immunotherapy.

Discussion

The capability of nanomedicines to deliver the therapeutics at the desired sites has brought distinct merits to cancer therapy. Great efforts have been devoted to overcome biological barriers via the engineering of carriers.[56–58] Hitchhiking strategy has been developed to improve the drug delivery efficacy, which is typically based on the ex vivo cell engineering technology.[6] In situ hitchhiking strategy to overcome the drawbacks of ex situ approach (e.g., short lifetime of cells and complex processes) holds great potential to simplify the delivery process.[13,18.19] Herein, we demonstrate the assembly of liposome-based vehicles functionalized with anti-Ly6G antibodies for hitchhiking delivery of DOX and STING agonist SR-717 via targeting NEs. After tumor resection, inflammatory factors are released to recruit the migration of inflammatory cells (e.g., NEs) to the postsurgical sites. Targeting of liposomes to NEs potentiates the accumulation of therapeutics at the postsurgical sites for improved delivery efficacy.

Cancer cell-intrinsic STING pathway, which can be activated by chemotherapeutics-induced ICD, plays a vital role in antitumor immunity.[59,60] ICD biomarkers detection and DC maturation experiments confirmed that the delivery of DOX resulted in ICD and the release of tumor-specific antigens, which together with SR-717 could activate the STING pathway and stimulate DC maturation. Specifically, the treatment with DOX induced the release of immunogenic substances from tumor cells (e.g., DNA) to activate STING pathway at the tumor sites. SR-717 could further amplify the signals and recruit immune cells, which contributed to the continuous activation of STING pathway. In addition, the co-delivered DOX and SR-717 in tumor site could effectively relieve immunosuppressive tumor microenvironment by up-regulation of tumor suppressor inflammatory factors. The remodeling of immunosuppressive microenvironments attracted monocytes/macrophages, NK cells and dendritic cells, and promoted the recognition of T cells to inhibit tumor recurrence and metastasis after surgery.

In summary, a targeted hitchhiking delivery strategy was designed and verified for postsurgical chemo-immunotherapy. The surgical resection of tumor sites induced the inflammatory responses and the subsequent recruitment of NEs, where in situ targeting of TLipDS improves the accumulation of DOX and SR-717. The delivered DOX could not only inhibit tumor growth for chemotherapy but can also improve the tumor immunogenicity induced by ICD. The released immunogenic substances (e.g., dsDNA) could activate the STING pathway, and the delivered SR-717 could further amplify the signals to elicit tumor-specific T cell immunity. Notably, the TLipDS demonstrated the effective inhibition the growth of the metastatic melanoma due to the activation of specific antitumor immune memory after the treatment. The co-delivery of drugs and agonists via the targeted hitchhiking delivery strategy provides an important insight in the combined chemo-immunotherapy for postsurgical tumor recurrence and metastatic melanoma growth.

Materials and methods

Assembly of liposomes

LipD was assembled by a transmembrane ammonium sulfate gradient method. In brief, a lipid mixture of HSPC (75 mg), Chol (25 mg), and DSPE-PEG2000-Biotin (25 mg) at a molar ratio of 56:39:5 was dissolved in 10 mL of chloroform in a 250 mL flask and evaporated under reduced pressure to form a lipid membrane. Subsequently, 10 mL of ammonium sulfate solution (0.3 M) was added for rehydration with the assistance of ultrasonication. Subsequently, the liposomes were sequentially extruded through a high-pressure microfluidizer (Nano-Genizer-II, Genizer) four times at an operation pressure of 15000 psi, followed by dialysis with PBS buffer (10 mM) for 24 h. The obtained liposomes were mixed with 15 mg of DOX·HCl (dissolved in 2 mL of H_2O) and incubated at 60 °C for 30 min, followed by centrifugation (50,000 g, 40 min, 4 °C) to remove the free DOX. For the assembly of LipD without modification of biotin, the component of DSPE-PEG2000-Biotin was replaced with DSPE-PEG2000.

LipS was assembled by a film-dispersion method. Briefly, HSPC (75 mg), Chol (15 mg), DSPE-PEG2000-Biotin (27 mg) and SR-717 (15 mg) were dissolved in 20 mL of methanol in a 250 mL flask and evaporated under reduced pressure to form a thin film. Subsequently, 10 mL of PBS buffer (10 mM) was added for rehydration with the assistance of ultrasonication. The obtained liposomes were extruded through the high-pressure microfluidizer (NanoGenizer-II, Genizer) four times at an operation pressure of 15000 psi to obtain the biotin-modified LipS. For the assembly of LipS, the component of DSPE-PEG2000-Biotin was replaced with DSPE-PEG2000.

For the modification of targeted molecules, biotin-modified LipD or LipS (10 mg) dispersion was incubated with 1 mg of avidin for 12 h at 4 °C, followed by centrifugation (50,000 g, 40 min, 4 °C) to remove the unreacted avidin. Subsequently, avidin-modified LipD and LipS were further incubated with biotin-conjugated anti-Ly6G antibodies (0.2 mg) for 12 h at 4 °C, which resulted in the formation of TLipD and TLipS, respectively.

Tumor and surgical resection model

To establish a postsurgical B16 tumor-bearing mouse model, the mice were subcutaneously inoculated with B16 cells (1×10^6 cells per mouse). Once the tumor size was approximately 100 mm^3 (7 days after inoculation), ~80% of the tumor tissue was removed, followed by disinfection and suture of the wound. The postsurgical 4T1 tumor-bearing mouse model was established according to the postsurgical B16 tumor-bearing mouse model, and the amount of inoculated 4T1 cells were 1×10^6 cells per mouse.

Evaluation of NEs in blood and tumor tissues after surgery

Blood samples were collected at the predetermined time points after surgery, followed by dissection of the tumor tissues. The blood sample was lysed to remove erythrocytes, followed by centrifugation (652 g) for 5 min. The obtained cells were labeled with APC-CD45, PE/Cyanine 7-CD11b and FITC-Ly6G antibodies. The expression level of surface markers was detected by flow cytometry. To analyze the tumor infiltration of NEs, the residual tumor tissues were harvested and homogenized into cell suspensions, followed by filtration with a 200-mesh sieve and centrifugation (652 g) for 5 min. The obtained cells were labeled with anti-CD45, anti-CD11b and anti-Ly6G antibodies for further evaluation. Tumor tissues were also collected for histological staining.

Targeting of liposomes to NEs

Mouse blood were collected at 4 h postsurgery and lysed to remove erythrocytes. The obtained immune cells were seeded into 24-well plates at a density of 2×10^5 cells per well. TLipD and LipD (equivalent DOX concentration of 5 μg mL^{-1}) were incubated with cells for 4 h, followed by sequential staining with Hoechst 33342 and FITC-Ly6G antibodies. Subsequently, cells were washed with DPBS twice and analyzed by flow cytometer and CLSM (excitations for DOX and FITC at 495 nm, excitation for Hoechst 33342 at 358 nm).

For the evaluation of in vivo targeting behavior. The mice were subcutaneously inoculated with B16 cells (1×10^6 cells per mouse). Once the tumor size was approximately 100 mm^3 (7 days after inoculation), ~80% of the tumor tissue was removed, followed by disinfection and suture of the wound. At 4 h postsurgery, TLipD, and LipD (DOX dosage of 15 mg/kg) was subcutaneously injected into mice. Blood samples and tumor tissues were collected and processed at the predetermined time, followed by labeling with APC-CD45, PE/Cyanine7-CD11b and FITC-Ly6G antibodies for further detecting by flow cytometry.

Tumor targeting

ICG-loaded liposomes (LipICG and TLipICG) were assembled by a film-dispersion method according to the preparation of LipS. The component of SR-717 was replaced with ICG. At 4 h postsurgery, TLipICG and LipICG were intravenously injected into the tumor-bearing mice. The mice without surgery were set as the control group. At the predetermined time points (6, 12, and 24 h), the residual tumor tissues were harvested for ex vivo imaging and the average fluorescence intensity of the ICG signal was analyzed using Living Image Software. To investigate the infiltration of DOX, tumor tissues were dissected for histological staining at 12 h post-injection of LipD or TLipD.

Intercellular transportation of drugs from NEs to tumor cells

NEs (1×10^5 cells/mL), obtained from bone marrow cells, were seeded in a sterile tube and incubated with TLipD (equivalent DOX concentration of 50.0 μg mL^{-1}) for 1 h at 37 °C to obtain TLipD/NEs. B16 cells were seeded in an 8-well chamber slide (3×10^3 cells per well). After 12 h culture, B16 cells were incubated with the above TLipD/NEs (2×10^4 cells per well), followed by incubation with PMA for 4 h. Subsequently, the cells were gently washed with DPBS twice and stained with Hoechst 33342 before imaging using CLSM.

Cytotoxicity of TLipD against B16 cells

The in vitro cytotoxicity of TLipD against B16 cells was determined using an MTT assay. B16 cells were seeded into 96-well plates at a density of 1×10^4 cells per well. After cell attachment for 12 h, cells were incubated with different concentrations of TLipD or/and TLipS (equivalent DOX or SR-717 concentration of 0.6, 1.3, 2.5, 5.0, 10.0, and 20.0 μg mL^{-1}). After 48 h incubation, 10 μL of MTT solution (5 mg mL^{-1}) was added to each well and incubated for 4 h. The supernatant was removed and 100 μL of DMSO was added to dissolve formazan crystals, followed by characterization of the absorbance at 570 nm.

Detection of the ICD biomarkers

The ICD biomarkers (i.e., CRT and HMGB1) of tumor cells after treatment were examined according to previously reported method. Briefly, B16 cells were seeded into 24-well plates at a density of 1×10^5 cells per well and cultured for 12 h, followed by incubation with TLipD, TLipS or TLipDS (equivalent DOX/SR-717 concentration of 5 μg mL^{-1}) for 24 h. The cells were washed with DPBS twice and incubated with anti-CRT antibodies for 30 min. After washing with DPBS three times, the cells were incubated with AF488-conjugated secondary antibodies for 30 min, followed by analysis with flow cytometry.

For immunofluorescence imagining of CRT expression, B16 cells

(1×10^5 cells per well) were seeded in confocal dishes and cultured for 12 h, followed by incubation with TLipD, TLipS or TLipDS (equivalent DOX/SR-717 concentrations of 5 μg mL^{-1}) for 24 h. Subsequently, the cells were washed with DPBS twice and fixed with 4% paraformaldehyde. The cells were further incubated with anti-CRT antibodies for 30 min, followed by sequential incubation with AF488-conjugated secondary antibodies and Hoechst 33342 for 30 and 10 min, respectively, before imaging with CLSM.

Intracellular HMGB1 was examined using the ELISA kit. B16 cells were seeded into 24-well plates (1×10^5 cells per well) and cultured for 12 h followed by incubation with TLipS and TLipDS (equivalent DOX/SR-717 concentrations of 5 μg mL^{-1}) for 24 h. The content of HMGB1 in the supernatant of the medium was detected by the ELISA kit according to the manufacturer's instructions.

BDMC maturation

BMDCs were obtained from C57 female mice (6 week) and cultured in the complete RPMI 1640 medium containing GM-CSF (20 ng mL^{-1}) and IL-4 (10 ng mL^{-1}) for 6 days. On day 7, the immature BMDCs were seeded into 24-well plates at a density of 5×10^5 cells per well and incubated with the supernatant medium of B16 cells, which were pre-incubated with TLipD, TLipS or TLipDS (equivalent DOX/SR-717 concentrations of 5 μg mL^{-1}) for 24 h. After incubation for 24 h, BMDCs were stained with APC-CD11c, FITC-CD80 and PE/Cyanine7-CD86, followed by analysis with flow cytometry. The cytokines of IL-6 and TNF-α□in the medium were detected using ELISA kits according to the manufacturer's instructions.

In vivo antitumor study

B16 model

To investigate the therapeutic activity of the in situ hitchhiking strategy, a melanoma-bearing mouse model was established. Briefly, 1×10^6 B16 cells were transplanted into the right flanks of mice. On day 8, mice were randomly divided into five groups. Tumors in all groups were partially resected (~80%) to mimic residual foci after surgery. At 4 h postsurgery, TLipD, TLipS, LipDS, and TLipDS (DOX or SR-717 dosage of 15 mg/kg) were subcutaneously injected into mice. The body weight and tumor volume were monitored every 2 days and tumor sizes were calculated according to the following formula of $width^2 \times length \times 0.5$. On day 24, five of mice were euthanized to obtain the tumors for further analysis, and other mice were monitored for study the tumor recurrence the survial rates. Specifically, H&E and immunofluorescence staining of tumor sections were used to investigate the apoptosis and proliferation of tumor cells as well as the T cell infiltration in tumors. To evaluate the improvement of tumor immune microenvironments, the tumor tissues were cut into small pieces and mashed into a single cell suspension using a 40 μm-cell strainer. After lysing erythrocytes, T lymphocytes were stained with APC-CD3, FITC-CD4 and PE-CD8 antibodies. MDSCs were stained with APC-CD45, PE/Cyanine7-CD11b, and FITC-Gr1 antibodies. Tregs were stained with FITC-CD4 and PE-Foxp3 antibodies, followed by analysis with flow cytometry. To analyze the immune memory of the mice after the treatments, effector memory T cells (PE-$CD8^+$AF488-$CD62L^-$APC-$CD44^+$) were stained and analyzed by flow cytometry. To examine the systemic immune responses, DLNs were harvested on day 15 for further analysis. DCs (FITC-$CD11c^+$PE-$CD80^+$PE/Cyanine-$CD86^+$) in DLNs were stained and analyzed by flow cytometry.

4T1 model

Briefly, 1.5×10^6 4T1 cells were transplanted into the right flanks of mice. On day 8, mice were randomly divided into seven groups. Tumors in all groups were partially resected (~80%) to mimic residual foci after surgery. At 4 h postsurgery, PBS, SR-717, TLipS, DOX, TLipD, LipDS, and TLipDS (DOX or SR-717 dosage of 15 mg/kg) was subcutaneously injected into mice. The body weight and tumor volume were monitored every 3 days and tumor sizes were calculated according to the following formula of $width^2 \times length \times 0.5$. On day 23, tumors were harvested for further analysis. Specifically, H&E and immunofluorescence staining of tumor sections were used to investigate the apoptosis and proliferation of tumor cells. To evaluate the improvement of tumor immune microenvironments, the tumor tissues were cut into small pieces and mashed into a single cell suspension using a 40 μm-cell strainer. After lysing erythrocytes, T lymphocytes were stained with APC-CD3, FITC-CD4 and PE-CD8 antibodies and analyzed by flow cytometry. DCs (FITC-$CD11c^+$PE-$CD80^+$PE/Cyanine7-$CD86^+$) in tumors were stained and analyzed by flow cytometry. Heart, liver, spleen, lung, and kidney were sectioned into slices and stained with hematoxylin and eosin (H&E) for histological analysis.

Lung metastasis

To establish the metastatic lung tumor models in mice, B16 cells (1×10^6) were subcutaneously injected into the armpit of anterior limb of female C57BL/6 mice. On day 7, B16 cells (1×10^6) were intravenously injected into B16 tumor-bearing mice. On day 8, the mice were randomly divided into five groups for tumor surgery and intravenous injection of liposomes. Upon the completion of therapy, the survival rate of mice was monitored. The lungs were collected on day 18 post-injection of liposomes. The metastatic lesions in lungs were recorded and sectioned for H&E staining.

Statistical analysis

Statistical analyses were performed using GraphPad software Prism (Version 8). Two-sided Student's t-test and one-way ANOVA using Tukey's test were applied to compare the statistical significance of differences between the groups. The differences were considered to be statistically significant for a p value below 0.05.

Author Statement

All authors declare that they have confirmed their consent to authors' contributions to this article and approved the submitted version.

Declaration of Competing Interest

The authors declare that they have no known competing financial interests or personal relationships that could have appeared to influence the work reported in this paper.

Data Availability

Data will be made available on request.

Acknowledgements

This work was financially supported by the National Natural Science Foundation of China (22072075, 21872085, 22102088), the Innovation Project of Jinan Science and Technology Bureau (2020GXRC022), and the Natural Science Foundation of Shandong Province of China (ZR2021QB046). This work was performed in part at the Analytical Centre for Structural Constituent and Physical Property, and the Translational Medicine Core Facility of Advanced Medical Research Institute at Shandong University.

Author Contributions

Zhiliang Gao and Jiwei Cui designed the experiments. Zhiliang Gao, Hongning Sun, and Mengqi Li prepared nanomedicines. Zhiliang Gao, Ning Wang, Yuan Ma, and Xinyi Jiang performed in vitro and in vivo experiments. Yunlu Dai, Xinyi Jiang, Shilei Ni, Jingcheng Hao and Jiwei

Cui supervised the project. All authors discussed the results and prepared the manuscript.

Appendix A. Supporting information

Supplementary data associated with this article can be found in the online version at doi:10.1016/j.nantod.2023.102096.

References

[1] W. Fan, B. Yung, P. Huang, X. Chen, Nanotechnology for multimodal synergistic cancer therapy, Chem. Rev. 117 (2017) 13566–13638, https://doi.org/10.1021/acs.chemrev.7b00258.

[2] J. Shi, P.W. Kantoff, R. Wooster, O.C. Farokhzad, Cancer nanomedicine: progress, challenges and opportunities, Nat. Rev. Cancer 17 (2017) 20–37, https://doi.org/10.1038/nrc.2016.108.

[3] N. Jyotsana, Z. Zhang, L. Himmel, F. Yu, M. King, Minimal Dosing of Leukocyte Targeting TRAIL Decreases Triple-negative Breast Cancer Metastasis Following Tumor Resection, Sci. Adv. 5 (2019), eaaw4197, https://doi.org/10.1126/sciadv.aaw4197.

[4] W. Tang, Z. Zhen, M. Wang, H. Wang, Y.J. Chuang, W. Zhang, G.D. Wang, T. Todd, T. Cowger, H. Chen, L. Liu, Z. Li, J. Xie, Red Blood Cell-Facilitated Photodynamic Therapy for Cancer Treatment, Adv. Funct. Mater. 26 (2016) 1757–1768, https://doi.org/10.1002/adfm.201504803.

[5] Z. Gao, H. Zhu, X. Li, P. Zhang, M. Ashokkumar, F. Cavalieri, J. Hao, J. Cui, Sono-Polymerization of Poly(ethylene glycol)-Based Nanoparticles for Targeted Drug Delivery, ACS Macro Lett. 8 (2019) 1285–1290, https://doi.org/10.1021/acsmacrolett.9b00576.

[6] J. Xue, Z. Zhao, L. Zhang, L. Xue, S. Shen, Y. Wen, Z. Wei, L. Wang, L. Kong, H. Sun, Q. Ping, R. Mo, C. Zhang, Neutrophil-Mediated Anticancer Drug Delivery for Suppression of Postoperative Malignant Glioma Recurrence,, Nat. Nanotechnol. 12 (2017) 692–700, https://doi.org/10.1038/nnano.2017.54.

[7] L. Feng, C. Dou, Y. Xia, B. Li, M. Zhao, P. Yu, Y. Zheng, A.M. El-Toni, N.F. Atta, A. Galal, Y. Cheng, X. Cai, Y. Wang, F. Zhang, Neutrophil-like Cell-Membrane-Coated Nanozyme Therapy for Ischemic Brain Damage and Long-Term Neurological Functional Recovery, ACS Nano 15 (2021) 2263–2280, https://doi.org/10.1021/acsnano.0c07973.

[8] C. Gao, Q. Wang, J. Li, C. Kwong, J. Wei, B. Xie, S. Lu, S. Lee, R. Wang, In vivo Hitchhiking of Immune Cells by Intracellular Self-assembly of Bacteria-Mimetic Nanomedicine for Targeted Therapy of Melanoma,, Sci. Adv. 8 (2022) eabn180, https://doi.org/10.1126/sciadv.abn1805.

[9] Y. Bi, W. Duan, J. Chen, T. You, S. Li, W. Jiang, M. Li, G. Wang, X. Pan, J. Wu, D. Liu, J. Li, Y. Wang, Neutrophil Decoys with Anti-Inflammatory and Anti-Oxidative Properties Reduce Secondary Spinal Cord Injury and Improve Neurological Functional Recovery, Adv. Funct. Mater. 31 (2021) 2102912, https:// doi.org/10.1002/adfm.202102912.

[10] C. Wyatt Shields IV, M. Evans, L. Wang, N. Baugh, S. Iyer, D. Wu, Z. Zhao, A. Pusuluri, A. Ukidve, D. Pan, S. Mitragotri, Cellular Backpacks for Macrophage Immunotherapy, Sci. Adv. 6 (2020) eaaz657, https://doi.org/10.1126/sciadv.aaz6579.

[11] Z. Du, C. Liu, H. Song, P. Scott, Z. Liu, J. Ren, X. Qu, Neutrophil-Membrane-Directed Bioorthogonal Synthesis of Inflammation-Targeting Chiral Drugs, Chem 6 (2020) 2060–2072, https://doi.org/10.1016/j.chempr.2020.06.002.

[12] Y. Zhang, C. Wang, W. Li, W. Tian, C. Tang, L. Xue, Z. Lin, G. Liu, D. Liu, Y. Zhou, Q. Wang, X. Wang, L. Birnbaumer, Y. Yang, X. Li, C. Ju, C. Zhang, Neutrophil Cyto-Pharmaceuticals Suppressing Tumor Metastasis via Inhibiting Hypoxia-Inducible Factor-1alpha in Circulating Breast Cancer Cells, Adv. Healthc. Mater. 11 (2022), e2101761, https://doi.org/10.1002/adhm.202101761.

[13] Z. Li, Y. Wang, Y. Ding, L. Repp, G.S. Kwon, Q. Hu, Cell-Based Delivery Systems: Emerging Carriers for Immunotherapy. Adv. Funct. Mater. 31 (2021), 2100088 https://doi.org/10.1002/adfm.202100088.

[14] Y. Xu, X. Zhang, G. Hu, X. Wu, Y. Nie, H. Wu, D. Kong, X. Ning, Multistage Targeted "Photoactive Neutrophil" for Enhancing Synergistic Photo-Chemotherapy, Biomaterials 279 (2021), 121224, https://doi.org/10.1016/j.biomaterials.2021.121224.

[15] C. Ju, Y. Wen, L. Zhang, Q. Wang, L. Xue, J. Shen, C. Zhang, Neoadjuvant Chemotherapy Based on Active Ingredient/Human Neutrophils Cytopharmaceuticals with Radiotherapy for Gastric Cancer, Small 15 (2019), e1804191, https://doi.org/ 10.1002/smll.201804191.

[16] M. Li, S. Li, H. Zhou, X. Tang, Y. Wu, W. Jiang, Z. Tian, X. Zhou, X. Yang, Y. Wang, Chemotaxis-Driven Delivery of Nano-Pathogenoids for Complete Eradication of Tumors Post-Phototherapy, Nat. Commun. 11 (2020), 1126, https://doi.org/10.1038/s41467-020-14963-0.

[17] L. Tang, Z. Wang, Q. Mu, Z. Yu, O. Jacobson, L. Li, W. Yang, C. Huang, F. Kang, W. Fan, Y. Ma, M. Wang, Z. Zhou, X. Chen, Targeting Neutrophils for Enhanced Cancer Theranostic, Adv. Mater. 32 (2020), e2002739, https://doi.org/10.1002/adma.202002739.

[18] D. Chu, X. Dong, X. Shi, C. Zhang, Z. Wang, Neutrophil-Based Drug Delivery Systems, Adv. Mater. 30 (2018), e1706245, https://doi.org/10.1002/adma.201706245.

[19] Z. Mi, L. Guo, P. Liu, Y. Qi, Z. Feng, J. Liu, Z. He, X. Yang, S. Jiang, J. Wu, J. Ding, W. Zhou, P. Rong, Trojan Horse" Salmonella Enabling Tumor Homing of Silver Nanoparticles via Neutrophil Infiltration for Synergistic Tumor Therapy and Enhanced Biosafety, Nano Lett. 21 (2021) 414–423, https://doi.org/10.1021/acs.nanolett.0c03811.

[20] D. Chu, X. Dong, Q. Zhao, J. Gu, Z. Wang, Photosensitization Priming of Tumor Microenvironments Improves Delivery of Nanotherapeutics via Neutrophil Infiltration,, Adv. Mater. 29 (2017), 1701021, https://doi.org/10.1002/adma.201701021.

[21] Y. Yu, Q. Cheng, X. Ji, H. Chen, W. Zeng, X. Zeng, Y. Zhao, L. Mei, Engineered Drug-loaded Cellular Membrane Nanovesicles for Efficient Treatment of Postsurgical Cancer Recurrence and Metastasis,, Sci. Adv. 8 (2022), eadd3599, https://doi.org/10.1126/sciadv.add3599.

[22] D. Sun, J. Zhang, L. Wang, Z. Yu, C.M. O'Driscoll, J. Guo, Nanodelivery of Immunogenic Cell Death-inducers for Cancer Immunotherapy, Drug Discov. Today 26 (2021) 651–662, https://doi.org/10.1016/j.drudis.2020.11.029.

[23] L. Xie, J. Li, G. Wang, W. Sang, M. Xu, W. Li, J. Yan, Z. Zhang, Q. Zhao, Z. Yuan, Q. Fan, Y. Dai, Phototheranostic Metal-Phenolic Networks with Antiexosomal PD-L1 Enhanced Ferroptosis for Synergistic Immunotherapy, J. Am. Chem. Soc. 144 (2022) 787–797, https://doi.org/10.1021/jacs.1c09753.

[24] Y. Li, Z. Su, W. Zhao, X. Zhang, N. Momin, C. Zhang, K.D. Wittrup, Y. Dong, D. J. Irvine, R. Weiss, Multifunctional Oncolytic Nanoparticles Deliver Self-replicating IL-12 RNA to Eliminate Established Tumors and Prime Systemic Immunity, Nat. Cancer 1 (2020) 882–893, https://doi.org/10.1038/s43018-020-0095-6.

[25] W. Li, J. Yang, L. Luo, M. Jiang, B. Qin, H. Yin, C. Zhu, X. Yuan, J. Zhang, Z. Luo, Y. Du, Q. Li, Y. Lou, Y. Qiu, J. You, Targeting Photodynamic and Photothermal Therapy to the Endoplasmic Reticulum Enhances Immunogenic Cancer Cell Death, Nat. Commun. 10 (2019), 3349, https://doi.org/10.1038/s41467-019-11269-8.

[26] G. Kroemer, L. Galluzzi, O. Kepp, L. Zitvogel, Immunogenic cell death in cancer therapy, Annu. Rev. Immunol. 31 (2013) 51–72, https://doi.org/10.1146/annurev-immunol-032712-100008.

[27] H. Tian, G. Wang, W. Sang, L. Xie, Z. Zhang, W. Li, J. Yan, Y. Tian, J. Li, B. Li, Y. Dai, Manganese-Phenolic Nanoadjuvant Combines Sonodynamic Therapy with cGAS-STING Activation for Enhanced Cancer Immunotherapy, Nano Today 43 (2022), 101405, https://doi.org/10.1016/j.nantod.2022.101405.

[28] J. Yan, G. Wang, L. Xie, H. Tian, J. Li, B. Li, W. Sang, W. Li, Z. Zhang, Y. Dai, Engineering Radiosensitizer-Based Metal-Phenolic Networks Potentiate STING Pathway Activation for Advanced Radiotherapy, Adv. Mater. 34 (2022), e2105783, https://doi.org/10.1002/adma.202105783.

[29] S. Chattopadhyay, Y. Liu, Z. Fang, C. Lin, J. Lin, B. Yao, C.Jack Hu, Synthetic Immunogenic Cell Death Mediated by Intracellular Delivery of STING Agonist Nanoshells Enhances Anticancer Chemo-immunotherapy, Nano Lett. 20 (2020) 2246–2256, https://doi.org/10.1021/acs.nanolett.9b04094.

[30] Z. Deng, M. Xi, C. Zhang, X. Wu, Q. Li, C. Wang, H. Fang, G. Sun, Y. Zhang, G. Yang, Z. Liu, Biomineralized MnO_2 Nanoplatforms Mediated Delivery of Immune Checkpoint Inhibitors with STING Pathway Activation to Potentiate Cancer Radio-Immunotherapy, ACS Nano 17 (2023) 4495–4506, https://doi.org/10.1021/acsnano.2c10352.

[31] T. Li, R. Song, F. Sun, M. Saeed, X. Guo, Ji Ye, F. Chen, B. Hou, Q. Zhu, Y. Wang, C. Xie, L. Tang, Z. Xu, H. Xu, H. Yu, Bioinspired magnetic nanocomplexes amplifying STING activation of tumor-associated macrophages to potentiate cancer immunotherapy, Nano Today 43 (2022), 101400, https://doi.org/10.1016/j.nantod.2022.101400.

[32] W. Jiang, Y. Wang, J.A. Wargo, F.F. Lang, B.Y.S. Kim, Considerations for Designing Preclinical Cancer Immune Nanomedicine Studies, Nat. Nanotechnol. 16 (2021) 6–15, https://doi.org/10.1038/s41565-020-00817-9.

[33] Y. Zhang, S. Ma, X. Liu, Y. Xu, J. Zhao, X. Si, H. Li, Z. Huang, Z. Wang, Z. Tang, W. Song, X. Chen, Supramolecular Assembled Programmable Nanomedicine As In Situ Cancer Vaccine for Cancer Immunotherapy, Adv. Mater. 33 (2021), e2007293, https://doi.org/10.1002/adma.202007293.

[34] Q. Chen, J. Chen, Z. Yang, J. Xu, L. Xu, C. Liang, X. Han, Z. Liu, Nanoparticle-Enhanced Radiotherapy to Trigger Robust Cancer Immunotherapy, Adv. Mater. 31 (2019), e1802228, https://doi.org/10.1002/adma.201802228.

[35] Z. Liu, X. Xu, K. Liu, J. Zhang, D. Ding, R. Fu, Immunogenic Cell Death in Hematological Malignancy Therapy, Adv. Sci. 10 (2023), 2207475, https://doi.org/10.1002/advs.202207475.

[36] W. Jiang, W. Dong, M. Li, Z. Guo, Q. Wang, Y. Liu, Y. Bi, H. Zhou, Y. Wang, Nitric Oxide Induces Immunogenic Cell Death and Potentiates Cancer Immunotherapy, ACS Nano 16 (2022) 3881–3894, https://doi.org/10.1021/acsnano.1c09048.

[37] S. Li, Z. Hong, Z. Wang, F. Li, J. Mei, L. Huang, X. Lou, S. Zhao, L. Song, W. Chen, Q. Wang, H. Liu, Y. Cai, H. Yu, H. Xu, G. Zeng, Q. Wang, J. Zhu, X. Liu, N. Tan, C. Wang, The Cyclopeptide Astin C Specifically Inhibits the Innate Immune CDN Sensor STING,, Cell Rep. 25 (2018) 3405–3421, https://doi.org/10.1016/j.celrep.2018.11.097.

[38] B.T. Roembke, J. Zhou, Y. Zheng, D. Sayre, A. Lizardo, L. Bernard, H.O. Sintim, A Cyclic Dinucleotide Containing 2-Aminopurine is A General Fluorescent Sensor for c-di-GMP and 3′,3′-cGAMP, Mol. Biosyst. 10 (2014) 1568–1575, https://doi.org/10.1039/c3mb70518h.

[39] J. Woodward, A. Iavarone, D. Portnoy, c-di-AMP Secreted by Intracellular Listeria Monocytogenes Activates a Host Type I Active Ingredient Response, Science 328 (2010) 1703–1705, https://doi.org/10.1126/science.1189801.

[40] L. Sun, J. Wu, F. Du, X. Chen, Z. Chen, Cyclic GMP-AMP Synthase is a Cytosolic DNA Sensor that Activates the Type I Active Ingredient Pathway, Science 339 (2013) 786–791, https://doi.org/10.1126/science.1232458.

[41] D. Shae, K. Becker, P. Christov, D. Yun, A. Lytton-Jean, S. Sevimli, M. Ascano, M. Kelley, D. Johnson, J. Balko, J. Wilson, Endosomolytic Polymersomes Increase the Activity of Cyclic Dinucleotide STING Agonists to Enhance Cancer Immunotherapy, Nat. Nanotechnol. 14 (2019) 269–278, https://doi.org/10.1038/s41565-018-0342-5.

[42] B.S. Pan, S.A. Perera, J.A. Piesvaux, J.P. Presland, G.K. Schroeder, J.N. Cumming, B.W. Trotter, M.D. Altman, A.V. Buevich, B. Cash, S. Cemerski, W. Chang, Y. Chen, P.J. Dandliker, G. Feng, A. Haidle, T. Henderson, J. Jewell, I. Kariv, I. Knemeyer, J. Kopinja, B.M. Lacey, J. Laskey, C.A. Lesburg, R. Liang, B.J. Long, M. Lu, Y. Ma, E. C. Minnihan, G. O'Donnell, R. Otte, L. Price, L. Rakhilina, B. Sauvagnat, S. Sharma, S. Tyagarajan, H. Woo, D.F. Wyss, S. Xu, D.J. Bennett, G.H. Addona, An Orally Available Non-Nucleotide STING Agonist with Antitumor Activity, Science 369 (2020), eaba6098, https://doi.org/10.1126/science.aba6098.

[43] E.N. Chin, C. Yu, V.F. Vartabedian, Y. Jia, M. Kumar, A.M. Gamo, W. Vernier, S. H. Ali, M. Kissai, D.C. Lazar, N. Nguyen, L.E. Pereira, B. Benish, A.K. Woods, S. B. Joseph, A. Chu, K.A. Johnson, P.N. Sander, F. Martínez-Peña, E.N. Hampton, T. S. Young, D.W. Wolan, A.K. Chatterjee, P.G. Schultz, H.M. Petrassi, J.R. Teijaro, L. L. Lairson, Antitumor Activity of a Systemic STING-Activating Non-Nucleotide cGAMP Mimetic, Science 369 (2020) 993–999, https://doi.org/10.1126/science.abb4255.

[44] Y. Tian, Z. Gao, N. Wang, M. Hu, Y. Ju, Q. Li, F. Caruso, J. Hao, J. Cui, Engineering Poly(ethylene glycol) Nanoparticles for Accelerated Blood Clearance Inhibition and Targeted Drug Delivery, J. Am. Chem. Soc. 144 (2022) 18419–18428, https://doi.org/10.1021/jacs.2c06877.

[45] H. Cai, L. Yan, N. Liu, M. Xu, H. Cai, IFI16 Promotes Cervical Cancer Progression by Upregulating PD-L1 in Immunomicroenvironment Through STING-TBK1-NF-kB Pathway, Biomed. Pharmacother. 123 (2020), 109790, https://doi.org/10.1016/j.biopha.2019.109790.

[46] Y. Xu, Y. Guo, C. Zhang, M. Zhan, L. Jia, S. Song, C. Jiang, M. Shen, X. Shi, Fibronectin-Coated Metal-Phenolic Networks for Cooperative Tumor Chemo-/Chemodynamic/Immune Therapy via Enhanced Ferroptosis-Mediated Immunogenic Cell Death, ACS Nano 16 (2022) 984–996, https://doi.org/10.1021/acsnano.1c08585.

[47] S. Chen, D. Li, X. Du, X. He, M. Huang, Y. Wang, X. Yang, J. Wang, Carrier-Free Nanoassembly of Active Ingredient Prodrug and siRNA for Combinationally Inducing Immunogenic Cell Death and Reversing Immunosuppression, Nano Today 35 (2020), 100924, https://doi.org/10.1016/j.nantod.2020.100924.

[48] G. Gao, Y. Jiang, W. Zhan, X. Liu, R. Tang, X. Sun, Y. Deng, L. Xu, G. Liang, Trident Molecule with Nanobrush–Nanoparticle–Nanofiber Transition Property Spatially Suppresses Tumor Metastasis, J. Am. Chem. Soc. 144 (2022) 11897–11910, https://doi.org/10.1021/jacs.2c05743.

[49] B. Wang, M. Tang, Z. Yuan, Z. Li, B. Hu, X. Bai, J. Chu, X. Xu, X.Q. Zhang, Targeted Delivery of a STING Agonist to Brain Tumors Using Bioengineered Protein Nanoparticles for Enhanced Immunotherapy,, Bioact. Mater. 16 (2022) 232–248, https://doi.org/10.1016/j.bioactmat.2022.02.026.

[50] M. Mamuti, Y. Wang, Y.D. Zhao, J.Q. Wang, J. Wang, Y.L. Fan, W.Y. Xiao, D. Y. Hou, J. Yang, R. Zheng, H.W. An, H. Wang, A Polyvalent Peptide CD40 Nanoagonist for Targeted Modulation of Dendritic Cells and Amplified Cancer Immunotherapy, Adv. Mater. (2022), e2109432, https://doi.org/10.1002/adma.202109432.

[51] M. Hu, L. Huang, Strategies targeting tumor immune and stromal microenvironment and their clinical relevance, Adv. Drug Deliv. Rev. 183 (2022), 114137, https://doi.org/10.1016/j.addr.2022.114137.

[52] E. Dai, Z. Zhu, S. Wahed, Z. Qu, W.J. Storkus, Z.S. Guo, Epigenetic Modulation of Antitumor Immunity for Improved Cancer Immunotherapy, Mol. Cancer 20 (2021), 171, https://doi.org/10.1186/s12943-021-01464-x.

[53] A. Pugazhendhi, T. Edisonb, B. Velmuruganc, J. Jacobd, I. Karuppusamye, Toxicity of Active Ingredient (Dox) to Different Experimental Organ Systems, Life Sci. 200 (2018) 26–30, https://doi.org/10.1016/j.lfs.2018.03.023.

[54] C. Xiang, Y. Yan, D. Zhang, Alleviation of the Active Ingredient-induced Nephrotoxicity by Fasudil in vivo and in vitro, J. Pharm. Sci. 145 (2021) 6–15, https://doi.org/ 10.1016/j.jphs.2020.10.002.

[55] S. Jhunjhunwala, C. Hammer, L. Delamarre, Antigen Presentation in Cancer: Insights into Tumour Immunogenicity and Immune Evasion, Nat. Rev. Cancer 21 (2021) 298–312, https://doi.org/10.1038/s41568-021-00339-z.

[56] S. Wang, X. Guo, W. Xiu, Y. Liu, L. Ren, H. Xiao, F. Yang, Y. Gao, C. Xu, L. Wang, Accelerating Thrombolysis Using a Precision and Clot-penetrating Drug Delivery Strategy by Nanoparticle-Shelled Microbubbles, Sci. Adv. 6 (2020), eaaz8204, https://doi.org/10.1126/sciadv.aaz8204.

[57] S. Chen, Y. Zhong, W. Fan, J. Xiang, G. Wang, Q. Zhou, J. Wang, Y. Geng, R. Sun, Z. Zhang, Y. Piao, J. Wang, J. Zhuo, H. Cong, H. Jiang, J. Ling, Z. Li, D. Yang, X. Yao, X. Xu, Z. Zhou, J. Tang, Y. Shen, Enhanced Tumour Penetration and Prolonged Circulation in Blood of Polyzwitterion-Drug Conjugates with Cell-Membrane Affinity, Nat. Bio. Eng. 5 (2021) 1019–1037, https://doi.org/10.1038/s41551-021-00701-4.

[58] H. Li, J. Du, X. Du, C. Xu, C. Sun, H. Wang, Z. Cao, X. Yang, Y. Zhu, S. Nie, J. Wang, Stimuli-Responsive Clustered Nanoparticles for Improved Tumor Penetration and Therapeutic Efficacy, Proc. Natl. Acad. Sci. USA 113 (2016) 4164–4169, https://doi.org/10.1073/pnas.1522080113.

[59] S. Li, W. Yu, F. Xie, H. Luo, Z. Liu, W. Lv, D. Shi, D. Yu, P. Gao, C. Chen, M. Wei, W. Zhou, J. Wang, Z. Zhao, X. Dai, Q. Xu, X. Zhang, M. Huang, K. Huang, J. Wang, J. Li, L. Sheng, L. Liu, Neoadjuvant Therapy with Immune Checkpoint Blockade, Antiangiogenesis, and Chemotherapy for Locally Advanced Gastric Cancer, Nat. Commun. 14 (2023), 8, https://doi.org/10.1038/s41467-022-35431-x.

[60] H. Guo, J. Huang, Y. Tan, W. Wu, T. Huang, N. Zhang, S. Chen, C. Zhang, X. Xie, X. Shuai, M. Xu, Nanodrug Shows Spatiotemporally Controlled Release of Anti-PD-L1 Antibody and STING Agonist to Effectively Inhibit Tumor Progression After Radiofrequency Ablation, Nano Today 43 (2022) 10425, https://doi.org/10.1016/j.nantod.2022.101425.